Inorganic Chemistry

Article

pubs.acs.org/IC

Introducing a Large Polar Tetragonal Distortion into Ba-Doped $BiFeO_3$ by Low-Temperature Fluorination

Oliver Clemens,*[,†,§] Robert Kruk,[§] Eric A. Patterson,[‡] Christoph Loho,[†] Christian Reitz,[§] Adrian J. Wright,[∥] Kevin S. Knight,[⊥] Horst Hahn,[†,§] and Peter R. Slater[∥]

[†]Joint Research Laboratory Nanomaterials and [‡]Institute of Materials Science, Technische Universität Darmstadt, Jovanka-Bontschits-Straße 2, 64287 Darmstadt, Germany

[§]Institute of Nanotechnology, Karlsruhe Institute of Technology, Hermann-von-Helmholtz-Platz 1, 76344 Eggenstein-Leopoldshafen, Germany

[∥]School of Chemistry, University of Birmingham, Edgbaston, Birmingham B15 2TT, United Kingdom

[⊥]ISIS Facility, Rutherford Appleton Laboratory, Harwell Oxford, Didcot OX11 0QX, United Kingdom

Supporting Information

ABSTRACT: This article reports on the synthesis and crystallographic and magnetic structure of barium-doped $BiFeO_3$ compounds with approximate composition $Bi_{1-x}Ba_xFeO_{3-x/2}$, as well as those of the fluorinated compounds $Bi_{1-x}Ba_xFeO_{3-x}F_x$ (both with x = 0.2, 0.3), prepared by low-temperature fluorination of the oxide precursors using polyvinylidenedifluoride. Whereas the oxide compounds were obtained as cubic (x = 0.2) and slightly tetragonal (x = 0.3, $c/a \approx 1.003$) distorted perovskite compounds, a large tetragonal polar distortion was observed for the oxyfluoride compounds ($c/a \approx 1.08$ for x = 0.2 and ~1.05 for x = 0.3), being isostructural to tetragonal $PbTiO_3$. Although described differently in previous reports on Ba-doped $BiFeO_3$, the observed remanent magnetization is found to agree well with the amount of $BaFe_{12}O_{19}$ only detectable by neutron diffraction and the well-known magnetic properties of $BaFe_{12}O_{19}$. The oxyfluoride compounds show G-type antiferromagnetic ordering with magnetic moments lying in the a/b plane.

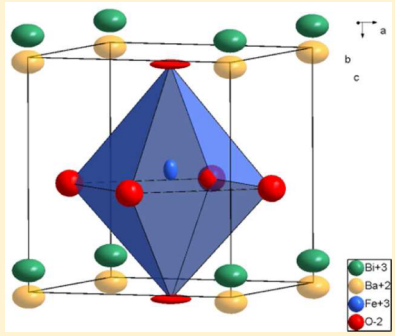

1. INTRODUCTION

Piezoelectric, particular ferroelectric materials are important in many devices,[1] with $Pb(Ti,Zr)O_3$ being the dominant choice in industrial applications such as inkjet printers, gas igniters, micropositioning systems, sonar, medical ultrasonic transducers, or actuators for fuel injection.[2,3] However, for toxicological reasons there is high interest in making lead-free perovskite-based ferroelectric piezoceramics[4,5] using highly abundant, environmentally friendly, low-cost elements. In this respect various solid solutions of bismuth-based compounds, such as $Bi_{0.5}Na_{0.5}TiO_3$, $Bi_{0.5}K_{0.5}TiO_3$, or $BiFeO_3$ have been widely studied.[6−10] In the case of $BiFeO_3$, it is of significant interest but generally has an intrinsic conductivity that is too high to be useful.[11] In the past decade, this material gained broader interest for its multiferroic properties, which potentially make it attractive in the field of data storage.[12−18] Both ferroelectric and antiferromagnetic ordering of $BiFeO_3$ are stable with Curie and Néel temperatures of 1098 and 643 K.[11]

The structure of $BiFeO_3$ can be derived from the cubic perovskite structure. Under ambient conditions, the compound crystallizes in the trigonal polar space group $R3c$ and shows spiral antiferromagnetic ordering.[19] It has been reported that the crystal structure can be affected by chemical doping as well as by introducing strain when preparing the material in thin film form. Usually, attempts to replace Bi^{3+} by a lower-valent alkaline earth ion AE^{2+} (resulting in the formation of vacancies at the same time following a composition of $Bi_{1-x}AE_xFeO_{3-x/2}$)[20−25] or by isovalent La^{3+} (to form $Bi_{1-x}La_xFeO_3$)[26,27] leads to transformation to a (pseudo)cubic perovskite compound with increasing amount of the dopant. Note that although the cubic space group is centrosymmetric, and thus theoretically prohibitive for the adaptation of a ferroelectric polarization, the local symmetry has been shown to be lower for a variety of compounds[28−32]. A change from trigonal to tetragonal was reported for the preparation of compounds of the system $BiFeO_3$−$PbTiO_3$; that is, by codoping $BiFeO_3$ on the A and B site with Pb^{2+} and Ti^{4+} ions, respectively,[33] a single-phase material with a large c/a ratio of ~1.19 was observed.

For the preparation of thin films, the substrate and the deposition condition has been shown to be highly influential in determining the kind of distortion induced by the perovskite compound. Theoretical calculations predict the formation of a tetragonal $P4mm$-type distortion only for conditions that induce a high degree of strain for pure $BiFeO_3$.[14] By this approach, a large tetragonal splitting with a c/a ratio of ~1.25 can be induced for thin films deposited on $SrTiO_3$, which is

Received: September 10, 2014
Published: November 10, 2014

   dx.doi.org/10.1021/ic502183t | Inorg. Chem. 2014, 53, 12572−12583

often described as supertetragonal. In addition, it was shown that chemical substitution of Bi^{3+} for Ba^{2+} can also introduce a tetragonal distortion in thin films at far lower strains,[34] and also A-site doping using neodymium has been shown to be successful in this respect.[35] Furthermore, Iliev et al. reported that supertetragonal $BiFeO_3$ should be favorable in terms of higher ferroelectric polarization values and simpler switching properties.[36] So far, no tetragonal *P4mm*-type $AFeX_3$ type phase (A = mainly Bi^{3+}, X = mainly oxygen) has been reported apart from thin-film preparations, and computational results indicate that such a phase should be energetically less stable.[14]

Topochemical manipulations are important reaction types especially in the field of battery-type materials[37−39] and for switchable material properties.[40] They are widely studied reaction types for directing structure properties of perovskite-type materials.[41] Among them, low-temperature fluorination reactions[42−44] are viable tools to influence the composition of the anion sublattice, to alter material properties (such as the introduction of superconductivity[45−47]) as well as to study the effect on magnetic structures and behavior,[48,49] but they are also interesting from a purely structural point of view in terms of anion ordering, whose understanding "would be critical if we are to utilize anion substitutions effectively to tailor the properties of materials".[50] Such reactions are usually necessary (instead of simple high-temperature reactions, which only work for few compounds for low fluoride contents[51−55]) due to the high stability of the alkaline earth fluorides AEF_2 and lanthanide oxyfluorides LnOF. A variety of fluorination agents have been used for such topochemical reactions, among them F_2, NH_4F, MF_2 (M = Cu, Zn), XeF_2 (see refs 56 and 44 for an overview), and it was recently shown that topochemical fluorination reactions can even be performed using electrochemical methods.[57] However, for the preparation of iron-containing oxyfluoride perovskites, polyvinylidenedifluoride (PVDF)[56] has proved to be a viable fluorination agent, and the compounds $SrFeO_2F$,[58,59] $BaFeO_2F$ (so far known in three different modifications),[60−63] $Sr_{1-x}Ba_xFeO_2F$[64], and $La_{1-x}Sr_xFeO_{3-x}F_x$[65,66] have all been synthesized using this fluorine-containing precursor. For all these systems (and also Fe-containing Ruddlesden−Popper-type phases prepared using PVDF[67]), the minimum Fe oxidation state was found to be Fe^{3+}, and no compounds with higher fluorine contents than the ones needed to obtain single-valent Fe^{3+} only have been reported so far (i.e., subsequent further reductive substitution of 1 O^{2-} by 1 F^{-}[44]). Therefore, if one wants to modify $BiFeO_3$ using PVDF, substitution of the Bi^{3+} ion by lower-valent alkaline earth ions will be required to make this reaction type applicable.

In this article we report on the first synthesis of tetragonal (*P4mm*-type) $Bi_{1-x}Ba_xFeO_{3-x}F_x$ (x = 0.2, 0.3) with a structure similar to $PbTiO_3$ as a bulk powder, showing a large c/a ratio of ∼1.08−1.05. The compounds were synthesized by solid-state reaction to prepare the precursor oxides and subsequent topochemical fluorination of the oxides using PVDF at reduced temperatures. So far, these are the first perovskite-type ferrite compounds containing only Fe^{3+} on the B site and showing this structural arrangement. In addition, we report on the magnetic structure of the as-prepared oxide and oxyfluoride compounds, which show G-type order of the magnetic moments. Furthermore, the identification of the ferrimagnetic impurity phase $BaFe_{12}O_{19}$ by means of neutron powder diffraction will likely provide an important new insight into the remanent magnetization found for Ba-doped $BiFeO_3$, which has been previously described as an intrinsic property of this phase.[68,21]

2. EXPERIMENTAL SECTION

2.1. Synthesis of Compounds. Approximately 4 g of samples of composition $Bi_{1-x}Ba_xFeO_{3-x/2}$ (x = 0.2, 0.3) were synthesized by conventional solid-state reactions. Stoichiometric amounts of starting powders of $BaCO_3$ (Sigma-Aldrich, ≥99%), Bi_2O_3 (Fluka, > 98%), and Fe_2O_3 (Fluka, ≥ 99%) were ground in a planetary ball mill (Retsch PM 100 CM, 300 rpm, 1 h) using isopropanol as dispergent. The samples were then heated at temperatures of 850 and 880 °C for 15 h, with a regrinding before each further heat treatment. For x = 0.3, the sample was heated a third time at 920 °C for another 15 h, since Ba-richer compounds are known to require higher reaction temperatures.[68,69,21] All heat treatments were performed in covered alumina crucibles without using an excess of Bi_2O_3.

Fluorination was achieved by grinding the as-synthesized powders with stoichiometric amounts of PVDF (Aldrich) in a 20% excess (i.e., 1:0.6 molar ratio of x in $Bi_{1-x}Ba_xFeO_{3-x}F_x/CH_2CF_2$ monomer unit), followed by slowly heating the mixture to a temperature of 370 °C for 15 h again using covered alumina crucibles.

2.2. Diffraction Experiments. X-ray powder diffraction (XRD) patterns of the oxide and oxyfluoride compounds were recorded on a Bruker D8 diffractometer with Bragg−Brentano geometry and a fine focus X-ray tube with Cu anode. No primary beam monochromator was attached. A VANTEC detector and a fixed divergence slit (0.1°) were used. The total scan time was 10 h for the angular range between 5 and 130° 2θ.

High-temperature XRD patterns of the oxyfluoride compounds were recorded on the same setup (except for using a 0.3° fixed divergence slit) using an Anton Paar HTK 1200N High-Temperature Oven-Chamber in a temperature range between 50 and 550 °C with a scan time of 1.5 h per scan.

Time of flight powder neutron diffraction (NPD) data were recorded on the HRPD high resolution diffractometer at the ISIS pulsed spallation source (Rutherford Appleton Laboratory, U.K.). Four grams of powdered samples were loaded into 8 mm diameter thin-walled, cylindrical vanadium sample cans, and data were collected at ambient temperature for 40 μAh proton beam current to the ISIS target (corresponding to ∼1 h beamtime) for the oxide compounds and for 80 μAh proton beam current to the ISIS target (corresponding to ∼2 h beamtime) for the oxyfluoride compounds.

Refinement of the magnetic and nuclear structure of $Bi_{1-x}Ba_xFeO_{3-x}F_x$ and $Bi_{1-x}Ba_xFeO_{3-x/2}$ (x = 0.2) was performed with the program TOPAS Academic 5[70,71] using the NPD data collected in all of the HRPD detector banks 1−3 at room temperature as well as the XRD data.

2.3. Magnetometric Measurements. Field-dependent direct current susceptibility measurements were performed using a Quantum Design MPMS-XL 5 SQUID magnetometer at 300 K between 0 and 4.8 T.

2.4. Mössbauer Measurements. The ^{57}Fe Mössbauer spectrum for $Bi_{0.7}Ba_{0.3}FeO_{2.7}F_{0.3}$ was recorded in standard transmission geometry in constant acceleration mode using a ca. 15 mCi ^{57}Co/Rh source at room temperature. The data are computed using the *WinNormos* software by R. A. Brand (WISSEL company).[72] The isomer shift is quoted relative to metallic iron at room temperature.

2.5. Scanning Electron Microscopy (SEM) and Energy Dispersive X-ray Spectroscopy (EDX). EDX spectra were recorded for $Bi_{1-x}Ba_xFeO_{3-x}F_x$ (x = 0.2, 0.3) using a Philips XL30 FEG scanning electron microscope operating at 30 keV. For EDX analysis the EDAX Genesis system was used, and an energy resolution of ∼140 eV was applied. The mapped area was on the order of 100 μm^2, and the atomic ratios were determined from the average of the Bi−M, Ba−L, and Fe−K lines, which were averaged over two spots of the sample. The samples were sputtered with approximately 10 nm of Au prior to the measurements.

2.6. Electrical Measurements. The sample powders were cold-isostatically pressed at 300 MPa (KIP 100 E, Paul-Otto Weber GmbH,

dx.doi.org/10.1021/ic502183t | Inorg. Chem. 2014, 53, 12572−12583

Table 1. Results of an EDX Analysis of $Bi_{1-x}Ba_xFeO_{3-x}F_x$ (x = 0.2, 0.3)

	x = 0.2			x = 0.3		
$Bi_{1-x}Ba_xFeO_{3-x}F_x$	theoretical	measured ± σ[a]	region of tolerance derived from σ	theoretical	measurement ± σ[a]	region of tolerance derived from σ
Fe–K	1	1 ± 0.02		1	1 ± 0.02	
Ba–L	0.2	0.22 ± 0.05		0.3	0.31 ± 0.05	
Bi–M	0.8	0.79 ± 0.01		0.7	0.65 ± 0.01	
ratio Bi/Ba	4.00	3.52	2.83–4.64	2.33	2.08	1.77–2.51
ratio Fe/Bi	1.25	1.27	1.23–1.31	1.43	1.55	1.49–1.61
ratio Fe/Ba	5.00	4.47	3.56–5.93	3.33	3.23	2.73–3.91

[a] σ was calculated from the intensity errors. The real σ is higher, since other sources of error (e.g., fit of background) would have to be taken into account.

Remshalden, Germany). Electrodes were applied using either Ag paint (G3692 Acheson Silver Dag 1415, Plano GmbH, Wetzlar, Germany) or Pt paint (Gwent Group Ltd., Pontypool, U.K.) and dried at 100 °C for 1 h. Temperature and frequency-dependent permittivity and impedance measurements were performed using an impedance analyzer (HP 4192A, Hewlett-Packard Co., Palo Alto, USA). For polarization measurements, the samples were first vacuum infiltrated with a silicone oil (AK 35, Wacker Chemie GmbH, München, Germany), which allowed the application of electric fields up to 6 kV/mm. For these polarization hysteresis measurements, a commercially available setup (aixPES system, aixACCT Systems GmbH, Aachen, Germany) was used. In this commercial system, polarization is measured according to the virtual ground method.

The reliable electrical characterization proved not to be possible due to the inability to sinter the samples without decomposition: the results from the attempted measurements are detailed in the Supporting Information.

3. RESULTS AND DISCUSSION

3.1. Analysis of the Nuclear and Magnetic Structure of $Bi_{1-x}Ba_xFeO_{3-x/2}$ (x = 0.2, 0.3) at Ambient Temperature. When synthesizing $BiFeO_3$-type compounds, it is known that the volatility of unreacted Bi_2O_3 at high temperature can cause the loss of large amounts of this component. Therefore, we attempted solid-state reaction after using high-energy ball milling to produce a reactive mixing of stoichiometric amounts of the oxide/carbonate precursors for the reaction. The ratios of the elements were confirmed to be correct within errors by an EDX analysis (see Table 1) of the fluorinated compounds $Bi_{1-x}Ba_xFeO_{3-x}F_x$ (x = 0.2, 0.3) (see Section 3.2.1). The cation ratio is unaffected by the fluorination due to the very low reaction temperatures (below 400 °C) and the fact that the fluorination reaction is a topochemical reaction. Although we cannot rule out small deviations from the ideal stoichiometry (e.g., following an equation $Bi_{1-x-d}Ba_{x+d}FeO_{3-(x+d)/2}/Bi_{1-x-d}Ba_{x+d}FeO_{3-x-d}F_{x+d}$), the general conclusions drawn in this article are independent of such small compositional deviations, and the excess of fluorination agent used is enough to compensate such compositional variations.

The as-synthesized oxide products were obtained as a (pseudo)cubic perovskite compound for x = 0.2, and a slightly tetragonal distorted perovskite compound for x = 0.3 ($c/a \approx$ 1.003, only detectable in the high-resolution NPD bank 1 data; also see comments on the tetragonal distortion found for $Bi_{0.5}Ba_{0.5}FeO_{2.75}$[73,74] later in this section). In the XRD patterns, a small amount of impurity of either tetragonal ß-Bi_2O_3 (x = 0.2, ~2 wt %), which is known to be stabilized by small degrees of doping,[75] and trigonal ~$Bi_{0.844}Ba_{0.156}O_{1.422}$[76] ($x$ = 0.3, ~4 wt %) were found, with no indication of further impurities being present. However, although undetectable in the XRD patterns, the presence of the ferrimagnetic compound $BaFe_{12}O_{19}$ at between 2 (x = 0.2) to 4 (x = 0.3) wt % was clearly indicated in the neutron diffraction patterns. Since this phase shows magnetic ordering up to high temperatures (T_C = 450 °C[77]), its magnetic reflections were also present in the pattern and could be described using the magnetic structure reported previously,[78] with a magnetic moment of ~4 μ_B per Fe^{3+} ion. The presence of $BaFe_{12}O_{19}$ is understandably far more difficult to be detected in the XRD data, which is reasonably explained by the fact that it contains mainly weaker scatterers compared to the main perovskite phase and also that its main reflection overlaps with the tails of the most intense (1 1 0) perovskite reflection. In contrast, the weaker neutron scatterers Bi_2O_3 and $Bi_{0.844}Ba_{0.156}O_{1.422}$ are very hard to detect in the neutron diffraction pattern (compared to phases containing the stronger scattering Fe atom), and their strongest neutron reflections additionally overlap with the perovskite reflections.

For the perovskite compound, magnetic reflections were found in the pattern, which can be indexed using a k-vector of [1/2 1/2 1/2]. Refinement of the magnetic structure of both compounds (x = 0.2 and 0.3) indicates G-type antiferromagnetic order with magnetic moments close to 3.74(2) μ_B (x = 0.2) and 3.70(2) μ_B (x = 0.3) per Fe atom. This value is similar in magnitude to those reported for other Fe^{3+}-containing perovskite compounds at room temperature.[55,62,66,63,79] Since a hypothetical canting moment would be very small (<0.1 μ_B per Fe atom) and due to the limited number of magnetic reflections present, such canting of the magnetic moment would be too small to be refined reliably from the NPD data. However, from the absence of further magnetic (superstructure) reflections or satellites, we conclude that the spiral magnetic order of $BiFeO_3$ is indeed destroyed by A-site doping with Ba^{2+}.[19]

No further reflections could be detected for x = 0.2 (neither in the XRD nor in the NPD data) apart from the ones belonging to the nuclear and magnetic phases reported above. For x = 0.3, one additional reflection at $d \approx$ 3.199 Å was detected but could not be assigned to one of the mentioned phases.

From XRD data alone, Khomchenko et al.[68,69,21,23] and Wang et al.[80] have reported that $Bi_{1-x}Ba_xFeO_{3-x/2}$ crystallizes in the trigonal space group $R3c$, being isotypic to the aristotype $BiFeO_3$. With regard to their diffraction patterns and/or reported trigonal lattice parameters, no superstructure reflections due to the lowering of symmetry from $Pm\bar{3}m$ to $R3c$ are visible in the patterns shown, and also the trigonal lattice parameters appear to be close to pseudocubic, approximately following the simple relation $c_{R3c} \approx a_{R3c}*6^{0.5}$. The Bi ion also does not shift far from its position for a pseudocubic arrangement of (0, 0, 1/4) with $z \approx$ 0.254 (compared to $z \approx$ 0.22 reported in ref 81). In contrast,

dx.doi.org/10.1021/ic502183t | Inorg. Chem. 2014, 53, 12572–12583

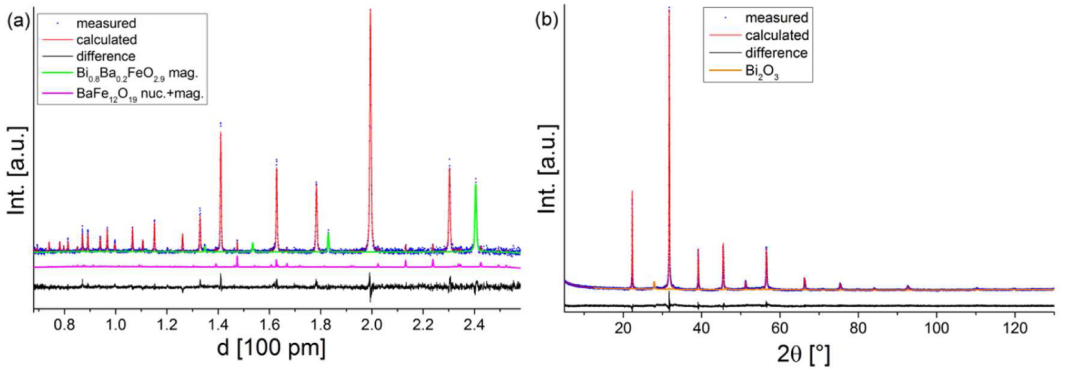

Figure 1. Rietveld analysis of the nuclear and magnetic structure of $Bi_{0.8}Ba_{0.2}FeO_{2.9}$. HRPD bank 1 (a) and XRD (b) data are shown. HRPD bank 2 and bank 3 data are provided as Figure S1a,b in the Supporting Information.

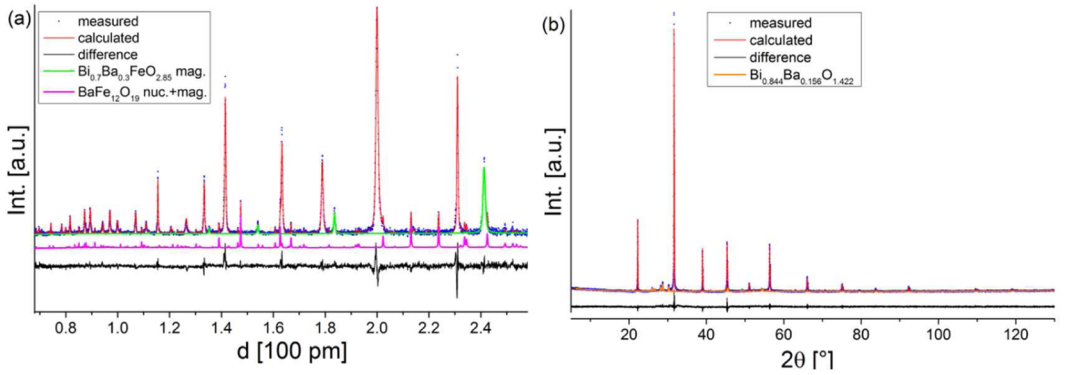

Figure 2. Rietveld analysis of the nuclear and magnetic structure of $Bi_{0.7}Ba_{0.3}FeO_{2.85}$. HRPD bank 1 (a) and XRD (b) data are shown. HRPD bank 2 and bank 3 data are provided as Figure S2a,b in the Supporting Information.

Table 2. Structural Parameters of the Compound with Nominal Composition $Bi_{0.8}Ba_{0.2}FeO_{2.9}$, Space Group *P4mm*, Z = 1

atom	atom type	site	*x*	*y*	*z*	occ.	$U_{1,1}$	$U_{3,3}$
Bi	Bi^{3+}	1a	0	0	−0.03(1)	0.8	0.086(4)	0.059(3)
Ba	Ba^{2+}	1a	0	0	0.06(8)	0.2		
Fe	Fe^{3+}	1b	1/2	1/2	0.5[a]	1	0.006(1)	0.031(3)
O	O^{-2}	1b	1/2	1/2	−0.01(1)	0.967	0.119(6)	0.050(6)
O	O^{-2}	2c	0	1/2	0.52(1)	0.967	0.006(1)	0.149(7)
a	3.9853(1)		*c*	3.9865(1)	R_{wp} (total)	11.3	R_{Bragg} [%] (XRD)	1.7
					GOF (total)	7.2	R_{Bragg} [%] (bank1)	3.2

[a]The position of the Fe ion was fixed to 0.5.

Table 3. Structural Parameters of the Compound with Nominal Composition $Bi_{0.7}Ba_{0.3}FeO_{2.85}$, Space Group *P4mm*, Z = 1

atom	atom type	site	*x*	*y*	*z*	occ.	$U_{1,1}$	$U_{3,3}$
Bi	Bi^{3+}	1a	0	0	−0.01(10)	0.7	0.065(2)	0.12(8)
Ba	Ba^{2+}	1a	0	0	0.01(10)	0.3		
Fe	Fe^{3+}	1b	1/2	1/2	0.5[a]	1	0.011(1)	0.028(3)
O	O^{-2}	1b	1/2	1/2	−0.01(3)	0.95	0.110(5)	0.05(2)
O	O^{-2}	2c	0	1/2	0.52(1)	0.95	0.007(1)	0.086(5)
a	3.9963(1)		*c*	4.0032(1)	R_{wp} (total)	10.7	R_{Bragg} [%] (XRD)	2.7
					GOF (total)	7.0	R_{Bragg} [%] (bank1)	2.9

[a]The position of the Fe ion was fixed to 0.5.

Dachraoui et al.[29] report on the formation of a cubic structure for $Bi_{0.81}Pb_{0.19}FeO_{2.905}$. However, by the use of TEM and from their structural analysis of synchrotron XRD data, it was found that the local symmetry is lower, with shifts of Bi ions along [1 1 0] or [1 1 1], and that the vacancy order cannot be considered to be random. In addition, the cubic space group was also reported for Ca-doped $BiFeO_3$ by Chen et al.[22]

A nonpolar tetragonal superstructure was reported for compositions close to $Bi_{0.5}Ba_{0.5}FeO_{2.75}$ by Boullay et al.[73,74] (space group *P4/mmm*, $c = 4*c_{primitive}$, $(c/a)_{primitive} \approx 1.02$), with superstructure reflections being clearly visible both in the XRD and NPD and showing additional incommensurate order. When preparing the oxides, we often found that a mixture of a tetragonal and a cubic phase was formed, for the first heating

dx.doi.org/10.1021/ic502183t | Inorg. Chem. 2014, 53, 12572−12583

instances, with the amount of the cubic phase increasing when heating to higher temperatures. We assume that this indicates a nonrandom distribution of the A site cations at lower temperatures, with Ba-richer regions belonging to the tetragonal phase observed by Boullay et al. and Bi-richer regions belonging to the cubic phase. Furthermore, such tetragonal phases are more likely to be found for compounds with increasing Ba content.

Plots of the Rietveld analyses are shown for $Bi_{0.8}Ba_{0.2}FeO_{2.9}$ and for $Bi_{0.8}Ba_{0.2}FeO_{2.9}$ in Figures 1 and 2; the structural data are listed for $Bi_{0.8}Ba_{0.2}FeO_{2.9}$ and for $Bi_{0.7}Ba_{0.3}FeO_{2.85}$ in Tables 2 and 3.

For both compounds, we tried to allow for displacement of the Bi and O ion along the [0 0 1], [0 1 1], and [1 1 1] directions. For all the directions, the shift away from the ideal cubic site was relatively small (far smaller compared to what we found for the fluorinated compounds described in Section 3.2.1 and also smaller compared to the standard deviation of the refined value), with thermal parameters of the A-site cations Bi and Ba being very high. This is in agreement with the general disorder on this site and could additionally indicate that Bi shifts away from its ideal position due to vacancies in its neighborhood (also see discussion of structural changes upon fluorination in Section 3.2.1). Since those vacancies are likely to be randomly (or nearly randomly) distributed (see Mössbauer studies reported in Section 3.4), this effect can be described by strong thermal motion for the Rietveld refinement. Both compounds were finally refined in the tetragonal space group *P4mm*, although it must be stated that especially for $x = 0.2$ the exact symmetry of this off-center shift remains questionable (the difference in lattice parameters is below the resolution limit of the diffraction data for this compound). It is worth mentioning that *P4mm* is a *translationengleiche* subgroup of *P4/mmm*, and therefore, also a *P4/mmm*-type structural distortion can be refined using this model (with the ions being then located on the ideal positions). Indeed, no indicative shifts away from the ideal positions could be observed for the Bi, Ba, and O ions, indicating that the assumption of an overall polar model of the compound is not correct, although the local symmetry is very likely to be reduced.

In addition, we found that the reflections of the perovskite phase showed anisotropic broadening (e.g., the (1 1 1) reflection and higher orders thereof suffer from the lowest broadening, similar to that reported by Dachraoui et al. for $Bi_{0.81}Pb_{0.19}FeO_{2.905}$[29]), and this was taken into account by using a model for anisotropic strain broadening utilizing spherical harmonics.

The presence of the ferrimagnetic compound $BaFe_{12}O_{19}$ makes a detailed discussion of any findings/changes of magnetic properties very difficult. We have shown here that small amounts of $BaFe_{12}O_{19}$ would be undetectable (or at least extremely difficult to detect) using laboratory-quality XRD data alone, even for very long measurement times, and that NPD can be used to show the presence of this phase even at these very small levels. However, since this compound can appear during synthesis, we believe that our findings offer a potential alternative explanation to the canting of spins reported by Khomchenko et al.[68,69,21,23] and Wang et al.,[80] who both used similar synthetic procedures compared to those we report in this article. In the case of the $Bi_{1-x}Ba_xFeO_{3-x/2}$ compounds reported here (and also of the $Bi_{1-x}Ba_xFeO_{3-x}F_x$ compounds reported in Section 3.2), the observed remanent magnetic moments fit very well to the amount of $BaFe_{12}O_{19}$ found on evaluation of the NPD data (and also to the magnitude of the magnetic moment reported by Khomchenko et al.,[68,69,21,23] the magnetization reported by Wang et al.[80] is higher by a factor of ∼4). This is shown by a detailed magnetic characterization and correlation with the diffraction experiments reported in Section 3.5. Keeping further in mind that the largest remanent magnetic moments were reported by Khomchenko et al. for Ba- and Pb-doping (compared to Ca- or Sr-doping) and increasing Ba/Pb content, and that for both compounds the ferrimagnetic phases $AFe_{12}O_{19}$ (A = Ba, Pb) are well-known, an extrinsic nature of the remanent magnetic moment might also plausibly explain the observation of remanent magnetic moments for A-site doped $BiFeO_3$. Such a presence of small amounts of $PbFe_{12}O_{19}$ was already assumed (although this compound was not detected by diffraction experiments) by Dachraoui et al. for $Bi_{0.81}Pb_{0.19}FeO_{2.905}$,[29] observing also a small remanent magnetic moment of ∼0.001 μ_B/f.u., similar to what was reported by Khomchenko et al.[68,69,21,23] (∼0.005 μ_B/f.u.).

3.2. Analysis of the Nuclear and Magnetic Structure of $Bi_{1-x}Ba_xFeO_{3-x}F_x$ (x = 0.2, 0.3) at Ambient Temperature. *3.2.1. Analysis of the Nuclear Structure of $Bi_{1-x}Ba_xFeO_{3-x}F_x$ (x = 0.2, 0.3).* The XRD patterns of the oxides in comparison to the oxyfluorides are shown in Figure 3.

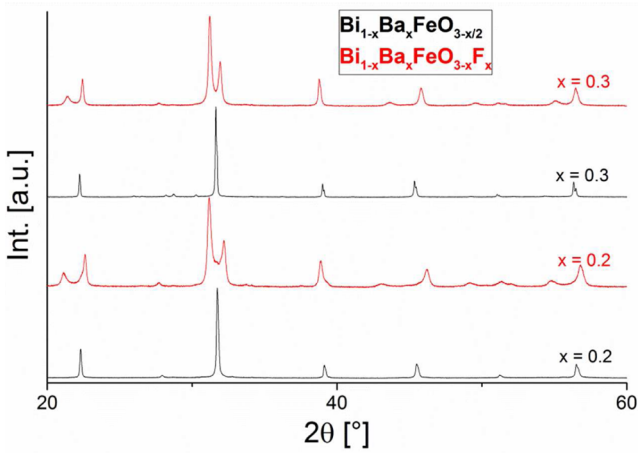

Figure 3. XRD patterns of the oxide and oxyfluoride compounds $Bi_{1-x}Ba_xFeO_{3-x/2}$ and $Bi_{1-x}Ba_xFeO_{3-x}F_x$.

It was found that a tetragonal distortion with a large c/a ratio is introduced into the material upon fluorination. The c/a ratio of 1.08 for $Bi_{0.8}Ba_{0.2}FeO_{2.8}F_{0.2}$ is also significantly higher than the value of 1.05 found for $Bi_{0.7}Ba_{0.3}FeO_{2.7}F_{0.3}$, agreeing well with the fact that the tetragonal distortion and its magnitude must be related to the ns^2 cation Bi^{3+}. The fluorination furthermore causes an increase of the cell volume for the oxyfluorides compared to the oxides of 1.4 Å^3 (x = 0.2) and 1.1 Å^3 (x = 0.3). This change in volume is not affected by change of oxidation state (as often observed for Fe-containing perovskites,[64,65] but ruled out from the Mössbauer measurements reported in Section 3.4, which confirm that the fluorinated compound $Bi_{0.7}Ba_{0.7}FeO_{2.7}F_{0.3}$ contains only Fe^{3+}), but is related to an increased anion interaction with the lone-pair (which is additionally accompanied by the tetragonal distortion).

Apart from the perovskite compound, a small impurity of BiOF was detected for both compositions, which is likely to be formed from the impurity of tetragonal Bi_2O_3 (or $Bi_{0.844}Ba_{0.156}O_{1.422}$) since the respective amounts compare very well. In the neutron diffraction pattern, the small amount of the

dx.doi.org/10.1021/ic502183t | Inorg. Chem. 2014, 53, 12572−12583

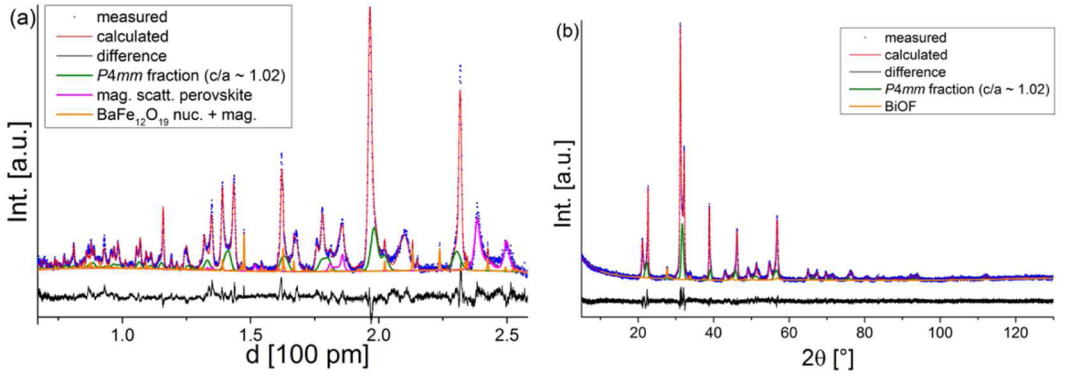

Figure 4. Rietveld analysis of the nuclear and magnetic structure of $Bi_{0.8}Ba_{0.2}FeO_{2.8}F_{0.2}$. HRPD bank 1 (a) and XRD (b). HRPD bank 1 (a) and XRD (b) data are shown. HRPD bank 2 and bank 3 data are provided as Figure S3a,b in the Supporting Information.

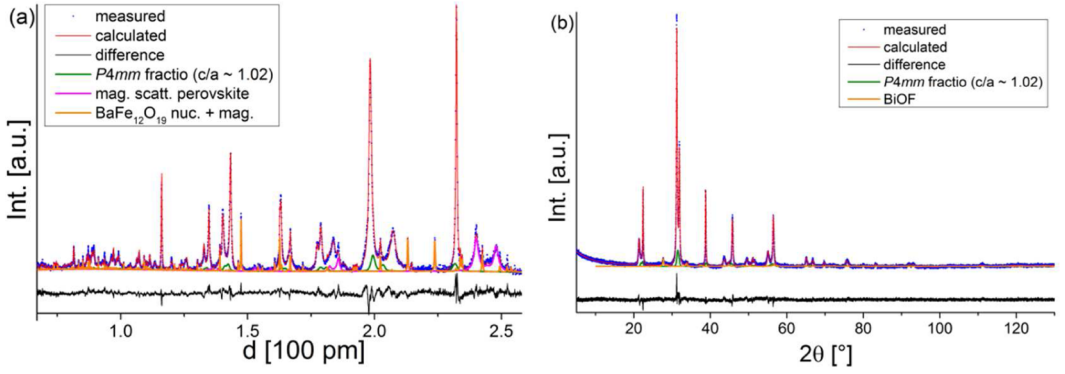

Figure 5. Rietveld analysis of the nuclear and magnetic structure of $Bi_{0.7}Ba_{0.3}FeO_{2.7}F_{0.3}$ (unknown reflection at d = 3.415−3.420 is marked with (*). HRPD bank 1 (a) and XRD (b) data are shown. HRPD bank 2 and bank 3 data are provided as Figure S4a,b in the Supporting Information.

ferrimagnetic impurity $BaFe_{12}O_{19}$ also present in the precursor oxide was found to be unaffected by the fluorination procedure.

$BaFe_{12}O_{19}$ is known for its ferrimagnetic properties. As for the pure oxides, we also found additional reflections that could be attributed to the magnetic scattering from the impurity phase $BaFe_{12}O_{19}$ and could be refined using the magnetic structure reported previously.[78]

To study the detailed crystallographic (and also magnetic structure, see Section 3.2.2), a combined Rietveld analysis of XRD and NPD data was performed. No superstructure reflections (apart from the magnetic reflections) or reflections not explained by the BiOF or $BaFe_{12}O_{19}$ impurity phases could be observed for x = 0.2, indicating that the nuclear structure can be refined on the basis of the smallest primitive perovskite cell with a_{nuc}, $c_{nuc} \approx 4$ Å. For x = 0.3 (but not for x = 0.2), we found one additional broad and small reflection (Figure 5b) in the bank 2 NPD data at $d \approx$ 3.415−3.420 Å (not present in the precursor oxide), which cannot be indexed on the basis of an ($2^{0.5}$ respectively 2)*$a_{primitive}$, ($2^{0.5}$ respectively 2)*$b_{primitive}$, (2 respectively 3 respectively 4)*$c_{primitive}$ unit cell, and is also not described by the superstructure reported by Boullay et al. for $Bi_{0.5}Ba_{0.5}FeO_{2.75}$ ($P4/mmm$, $c = 4*c_{primitive}$). However, the fact that no further reflections, for example, at d > 4 Å, could be observed, as well as that no further reflections were found in the XRD data, makes an assumption of an increased unit cell implausible and might indicate the presence of a further small amount of a potential decomposition product. For this size of unit cell, two tetragonal *translationengleiche* subgroups of the cubic space group $Pm\bar{3}m$ can be found, namely, the centrosymmetric space group $P4/mmm$ and the noncentrosymmetric space group $P4mm$. Whereas the space group $P4/mmm$ can be found for compounds with cations for which distortion of coordination polyhedron is influenced by the Jahn−Teller effect (e.g., $RbCuF_3$[82]), the polar space group $P4mm$ is well-known for perovskite compounds showing ferro- (and therefore also piezo- and pyro-) electric properties (e.g., $BaTiO_3$,[83] $Pb(Zr,Ti)O_3$,[84] and $PbTiO_3$[85]).

Comparing the fits to the neutron and X-ray diffraction patterns for both structural models, we found strong indication that the polar space group (compared to a model within the $P4/mmm$ space group allowing for shifts away from the ideal positions) must be considered to be the valid model. This difference of quality of fit for the two different space groups is clearly evident by eye in the XRD pattern and NPD bank 3 pattern (see Supporting Information, but also the ΔR_{wp}(total) = 1% and $\Delta R_{Bragg,\ individual}$(XRD, all NPD banks) ≈ 1% are very significant), indicating that the strongest scatterer Bi^{3+} is responsible most for this polar off-center displacement. The compound was therefore refined in the polar space group $P4mm$, and the fit to the diffraction patterns is shown for $Bi_{0.8}Ba_{0.2}FeO_{2.8}F_{0.2}$ in Figure 4 and for $Bi_{0.7}Ba_{0.3}FeO_{2.7}F_{0.3}$ in Figure 5. This is also confirmed applying Hamilton's R-test[86] on the R_{Bragg} values for the different models, which shows that the $P4/mmm$ model can be rejected at the 0.005 level (again see Supporting Information).

The widths of the reflections of the X-ray diffraction patterns and their angular dependence indicate the presence of both microstrain effects and crystallite size effects contribute significantly to reflection broadening. In addition, we also found that the (0 0 l) reflections are significantly broader than

dx.doi.org/10.1021/ic502183t | Inorg. Chem. 2014, 53, 12572−12583

Table 4. Structural Parameters of the Compound with Nominal Composition $Bi_{0.8}Ba_{0.2}FeO_{2.8}F_{0.2}$, Space Group *P4mm*, *Z* = 1

atom	atom type	site	*x*	*y*	*z*	occ.	$U_{1,1}$	$U_{3,3}$
Bi	Bi^{3+}	1a	0	0	−0.093(1)	0.8	0.043(1)	0.037(3)
Ba	Ba^{2+}	1a	0	0	0.010(8)	0.2		
Fe	Fe^{3+}	1b	1/2	1/2	0.5[a]	1	0.006(1)	0.016(1)
O/F1	O^{-2}/F^{-}	1b	1/2	1/2	0.043(1)	1	0.057(1)	0.003(2)
O/F2	O^{-2}/F^{-}	2c	0	1/2	0.570(1)	1	0.026(1)	0.024(2)
a	3.9276(1)		*c*	4.1926(2)	R_{wp} (total)	9.7	R_{Bragg} [%] (XRD)	1.6
$\varepsilon_{0,a}$ [%]	0.3		$\varepsilon_{0,c}$ [%]	1.1	GOF (total)	7.9	R_{Bragg} [%] (bank1)	5.0

[a]The position of the Fe ion was fixed to 0.5.

Table 5. Structural Parameters of the Compound with Nominal Composition $Bi_{0.7}Ba_{0.3}FeO_{2.7}F_{0.3}$, Space Group *P4mm*, *Z* = 1

atom	atom type	site	*x*	*y*	*z*	occ.	$U_{1,1}$	$U_{3,3}$
Bi	Bi^{3+}	1a	0	0	−0.090(1)	0.7	0.056(1)	0.044(4)
Ba	Ba^{2+}	1a	0	0	0.024(5)	0.3		
Fe	Fe^{3+}	1b	1/2	1/2	0.5[a]	1	0.009(1)	0.020(1)
O/F1	O^{-2}/F^{-}	1b	1/2	1/2	0.037(1)	1	0.047(1)	0.003(2)
O/F2	O^{-2}/F^{-}	2c	0	1/2	0.555(1)	1	0.022(1)	0.026(1)
a	3.9624(1)		*c*	4.1428(1)	R_{wp} (total)	9.2	R_{Bragg} [%] (XRD)	2.64
$\varepsilon_{0,a}$ [%]	0.4		$\varepsilon_{0,c}$ [%]	1.0	GOF (total)	6.9	R_{Bragg} [%] (bank1)	3.18

[a]The position of the Fe ion was fixed to 0.5.

the respective (h 0 0) reflections. Therefore, we introduced a model that allows for a more flexible refinement of reflection broadening for the two different crystallographic axes (again by the use of spherical harmonics). Furthermore, we estimated a sort of directional microstrain $\varepsilon_{0,a}$ and $\varepsilon_{0,c}$ by using a fit model with multiple perovskite phases with different lattice parameters (which we define as the fraction of the standard deviation of the lattice parameter to the mean lattice parameter) and found that $\varepsilon_{0,c}$ is nearly tripled compared to $\varepsilon_{0,a}$ (see Tables 4 and 5).

It must also be mentioned that we had to include a second fraction of the perovskite compound to refine the diffraction patterns properly. This is likely due to the tetragonal perovskite not only showing broadening due to strain, but that this broadening is also asymmetric, with slightly higher intensities for *c*/*a* ratios closer to 1 compared to *c*/*a* ratios above 1.08 (for $x = 0.2$) and 1.05 (for $x = 0.3$). These fractions are, however, found to be at a far lower level than the main tetragonal perovskite phase (i.e., in a ratio of ∼1:4 for $x = 0.2$ and ∼1:9 for $x = 0.3$), and show a significantly smaller *c*/*a* ratio of ∼1.02 for both compositions together with a slightly reduced cell volume by ∼1.4 Å^3 ($x = 0.2$) and ∼0.7 Å^3 ($x = 0.3$) compared to the main fraction. The cell volume of those fractions is more similar to the corresponding oxide phases; however, adding more PVDF and repeating the heating procedure did not result in "elimination" of this second perovskite-type phase. Possibly, this asymmetry can be explained by nonideal statistical distribution of the Ba^{2+} and Bi^{3+} ions and subsequent varying compositions in the grains. For this second phase, the same structural parameters as the main phase were used. Because of the minor influence of this phase and high reflection overlap, it is not possible to reliably refine structural parameters independently. Furthermore, attempts were made to refine the pattern with an *R*3*c* symmetry for the minor fraction; however, the obtained fit was significantly worse compared to using two tetragonal fractions ($\Delta R_{wp,total} \approx 1\%$).

The refined structural parameters for $Bi_{1-x}Ba_xFeO_{3-x}F_x$ are listed in Tables 4 and 5, and a drawing of the crystal structure is exemplarily shown for $x = 0.2$ in Figure 6 (both compounds are structurally very similar). $Bi_{1-x}Ba_xFeO_{3-x}F_x$ ($x = 0.2, 0.3$) show

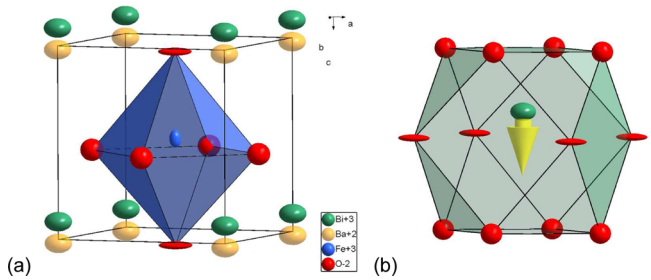

Figure 6. Refined crystal structure together with thermal ellipsoids for the different ions of $Bi_{0.8}Ba_{0.2}FeO_{2.8}F_{0.2}$ (a). The location of the Bi ion (green) in its anion (red) coordination polyhedron together with the mutual position (as found for $PbTiO_3$[87]) of the lone pair indicated by an yellow arrow (b) is shown. For a detailed analysis of the lone pair position, DFT-based calculations would be required.

a high similarity to the ferroelectric compound $PbTiO_3$; that is, the same kind of off-center shift for the ions by a similar magnitude was observed. In $PbTiO_3$ the lone pair of the ns^2 cation (Pb^{2+}) is known to be directed toward where the Ba ion is located in $Bi_{1-x}Ba_xFeO_{3-x}F_x$, and so in $Bi_{1-x}Ba_xFeO_{3-x}F_x$, a similar directional orientation of the lone pair must therefore also be considered to be highly likely (see Figure 6b).

The reasons for the introduction of tetragonal distortion on fluorination may relate to the displacive stereochemical activity of the lone pair being somehow suppressed in the Ba-doped $Bi_{1-x}Ba_xFeO_{3-x/2}$ oxide compounds but reactivated in the fluorinated compounds. It is known in the literature that the lone pair of the Bi^{3+} ion occupies approximately as much space as an oxide or fluoride anion in the crystal.[88,14] Therefore, on introduction of vacancies in the anion sublattice, the lone pair is likely to point toward such a vacancy for space reasons. This was already well-investigated in a density functional theory (DFT) study by Walsh et al. on the different modifications of Bi_2O_3;[89] for the oxygen disordered δ-modification of Bi_2O_3 it was found that the ns^2 cation forms a lone pair, pointing toward the oxygen vacancy, that is, the "region of space" in the crystal lattice. For perovskite compounds that show a random (or nearly random) distribution of the vacancies in the anion

dx.doi.org/10.1021/ic502183t | Inorg. Chem. 2014, 53, 12572−12583

sublattice (as found for $Bi_{1-x}Ba_xFeO_{3-x/2}$), a pseudocubic arrangement will have to form, and a uniform displacive ns^2 ion induced distortion will be simply suppressed.

On "refilling" of the anion sublattice with fluoride ions by substituting 1 O^{2-} for 2 F^-, the unidirectional displacive effect of the Bi^{3+} ion can be recovered over a large area of the crystallite (O^{2-} and F^- only differ by ∼0.06 Å for their ionic radii[90]), since the whole anion sublattice is now occupied by anions. This is in agreement with the increase of cell volume due to fluorination, since the additional anions will require the space that has previously been occupied by the lone pair in the oxide compounds. However, such an increase in cell volume does not necessarily accompany fluorination of Fe-containing perovskite compounds (where the average Fe oxidation state is maintained). For example, the vacancy-ordered monoclinically distorted perovskite compound $BaFeO_{2.5}$ reported by Clemens et al.[79] shows a decrease in cell volume on fluorination to $BaFeO_2F$. In contrast, the brownmillerite-type $SrFeO_{2.5}$ shows an increase in cell volume on fluorination to $SrFeO_2F$. These differences are explained by the differences in structural distortions in $BaFeO_{2.5}$ and $SrFeO_{2.5}$. Furthermore, if we consider that the volume changes per fluoride ion (−1.02 $Å^3/F^-$ for $BaFeO_{2.5}$ and 0.65 $Å^3/F^-$ for $SrFeO_{2.5}$) are significantly smaller than those for the fluorination of $Bi_{1-x}Ba_xFeO_{3-x}F_x$ (7 $Å^3/F^-$ for x = 0.2 and 3.7 $Å^3/F^-$ for x = 0.3), we can conclude that the space of the vacancy is likely to have been occupied by the lone pair of Bi^{3+} cations in the oxide compounds, which is well-known to act as a pseudoanion.[91]

Although the ns^0 cation Ba^{2+} does not participate in the off-center displacement and shifts toward the "ideal" position 0, 0, 0 in relation to the position of the Fe atom, the overall polar distortion remains stable in the fluorinated compounds. It must be mentioned at this point that a similar quality of fit was observed when fixing the Ba and Bi ion to the same position, which is refined to 0, 0, and ca. −0.07 then, without significant change of the positions of the other ions. However, since the refinement proved to be stable and converged properly using a split site for this compound (which would chemically make sense), we have given the split parameters in Tables 4 and 5.

The adaption of the tetragonal distortion is in contrast to what was found for La-doped $BiFeO_3$ compounds ($Bi_{1-x}La_xFeO_3$; isovalent substitution of Bi^{3+} by La^{3+}) for which a transformation toward a pseudocubic structure is obtained for a far lower degree of doping (∼x = 0.1 deduced from the diffraction patterns shown in ref 27). The difference in ionic radii between La^{3+} and Ba^{2+} is large (1.36 vs 1.61 Å for 12-fold coordination[90]), and it has already been shown that structural distortions found in the series $La_{1-x}Sr_xFeO_{3-x}F_x$ ($0 \leq x \leq 1$, also monovalent Fe^{3+} for all compositions) for increasing La content arise from the fact that the La^{3+} ion tries to lower its effective coordination number.[65,66] In contrast, a high thermal displacement parameter of the Fe atom was observed for $BaFeO_2F$, indicating that a local polar displacement is likely in this compound, although an overall cubic perovskite structure was observed.[60] Therefore, the larger Ba^{2+} and its compatibility with local 12-fold coordination might facilitate the formation of the polar tetragonal distortion for the compounds $Bi_{1-x}Ba_xFeO_{3-x}F_x$, whereas local structural distortions for La^{3+} would just be too strong to maintain the stereochemical activity of Bi^{3+} over larger crystallite sizes.

There also appears to be a clear difference for the $Bi_{1-x}Ba_xFeO_{3-x}F_x$ compounds (x = 0.2, 0.3) compared to $PbFeO_2F$, for which the larger F content and associated disorder of the O^{2-} and F^- ions might be prohibitive for the adoption of a uniform polar distortion (i.e., the compound is found in the cubic perovskite structure with strong displacement of the A site cations toward the 12 possible [1 1 0] like directions). So far, it is not entirely clear why $PbFeO_2F$ does not show stereochemical activity of the ns^2 cation Pb^{2+}.

From the shape of the thermal displacement ellipsoids shown in Figure 6a, a slight local tilting of the octahedra is also indicated for $Bi_{1-x}Ba_{1-x}FeO_{3-x}F_x$ (x = 0.2, 0.3) by the disclike shape of the thermal ellipsoid of the O/F1 ion, and blocks with different tilting in the a/b plane might be present. This would also be in good agreement with a tolerance factor of ∼0.92−0.94 calculated from the average ionic radii reported in 90 (estimating the radius of Bi^{3+} to 1.36 Å for 12-fold coordination by interpolation). However, it is worth mentioning that such a disclike thermal ellipsoid could also arise from the disorder on the A site and shifts of the oxygen ion away from the lone pair of Bi^{3+} toward a Ba^{2+} ion in the same plane. The slightly rodlike shape of the thermal ellipsoid of the Fe atom can be explained by a partial split position: for octahedra surrounded by a higher number of Ba^{2+} ions, the Fe ion is more likely to shift toward the center of the octahedron, whereas for octahedra surrounded by a higher number of Bi^{3+} ions, a shift away from this center toward one corner of the octahedron would be plausible.

Additionally, the direction-dependent broadening of the reflections is also in good agreement with the assumption of the lone pair pointing along the c-axis. Since the Bi^{3+} and the Ba^{2+} ion strongly differ in the shape of their electron shell (i.e., rodlike vs spherelike), this would cause a stronger fluctuation of the lattice plane distances along the direction in which the lone pair is pointing at, namely, the c-axis for $Bi_{1-x}Ba_xFeO_{3-x}F_x$.

It might be worth mentioning that attempts to synthesize oxyfluorides with a lower Ba content (i.e., lower values of x) did not result in the formation of phase-pure compounds although the precursor oxides appeared to be single-phase perovskite compounds. Instead, mixtures of two perovskite-type phases (trigonal $R3c$ and tetragonal $P4mm$) were observed. Since no single-phase products could be obtained, those compositions were not investigated further.

3.2.2. Analysis of the Magnetic Structure of $Bi_{1-x}Ba_xFeO_{3-x}F_x$ (x = 0.2, 0.3). Analysis of the magnetic reflections showed that they are compatible with a k-vector of [1/2 1/2 1/2]. Among the maximal magnetic subgroups of $P4mm$ allowing for this k-vector (determined using the program MAXMAGN[92] on the Bilbao Crystallographic Server[93−95]), only the groups 108.238 and 46.246 are compatible with a magnetic moment on the Fe atoms. The magnetic space group 108.238 is compatible with a G-type alignment of the magnetic moments along the c-axis, whereas 46.246 is compatible with G-type alignment of the magnetic moment along one of the crystallographic axes a or b. However, since the nuclear cell shows tetragonal symmetry only an overall magnetic moment lying in the a/b plane can be determined from powder diffraction data.[96] Both groups were tested, and a proper fit of the reflections could only be obtained for the space group 46.246 (I_cma2), with an overall magnetic moment of 3.7(1) μ_B per Fe atom. This magnetic moment is again in good agreement with what has been observed for other G-type ordered Fe^{3+}-containing perovskites at room temperature.[55,62,66,63,79] Furthermore, the alignment of the magnetic moment within the a/b plane was also found by Boullay et al.[73] for tetragonal $Bi_{0.5}Ba_{0.5}FeO_{2.75}$ ($P4/mmm$, $c = 4*c_{prim.}$). None of the maximal subgroups of $P4mm$ with k = [1/2 1/2 1/2] allow

dx.doi.org/10.1021/ic502183t | Inorg. Chem. 2014, 53, 12572−12583

for the presence of a permanent magnetic moment due to canting. We believe that the occurrence of the impurity $BaFe_{12}O_{19}$ explains the magnetic moment quite well (see Section 3.5), but if such a permanent magnetic moment would exist, it could either lie along the *c*-axis or even within the *a*/*b* plane. However, this is not indicated in fits using the magnetic space group 1.1 and applying proper constraints to the directions of the magnetic moments between different crystallographic sites (the canting moment would just be too small to be refined reliably), although such a very small canting moment cannot be ruled out entirely by the analysis of the NPD data.

3.3. High-Temperature X-ray Diffraction Experiments. High-temperature X-ray diffraction experiments were performed to determine the decomposition and phase transition behavior of the as-prepared oxyfluorides. We found that on heating the compounds to a temperature of approximately 400 °C, the tetragonal polar distortion remains stable, and the *c*/*a* ratio also stays nearly constant. On cooling the compounds to room temperature when not heated above 400 °C, we found that the lattice parameters match very well to what was found during the heating procedure (see Figure 7).

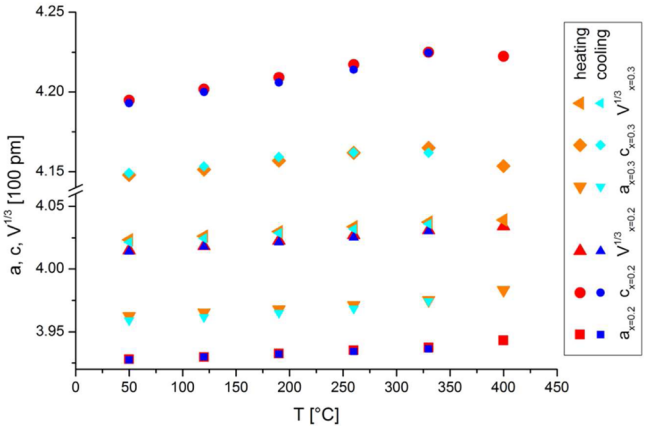

Figure 7. Temperature dependence of the tetragonal lattice parameters *a* and *c* as well as the cube root of the cell volume $V^{1/3}$ for heating $Bi_{1-x}Ba_xFeO_{3-x}F_x$ to 400 °C.

When heating the compound to temperatures above 400 °C, a change from tetragonal toward cubic was found. This structural change is accompanied by the formation of BaF_2, which is a well-known decomposition product for $BaFeO_2F$-type compounds[64,62,63] (also see end of this paragraph). On cooling from temperatures ≥450 °C, the tetragonal distortion was not found to be reappearing, highlighting that the use of topochemical reactions is inalienable for the preparation of oxyfluorides for compounds of the system $Bi_{1-x}Ba_xFeO_{3-x}F_x$ (see Supporting Information for the pattern of $Bi_{0.7}Ba_{0.3}FeO_{2.7}F_{0.3}$ heated at 550 °C in comparison to undecomposed $Bi_{0.7}Ba_{0.3}FeO_{2.7}F_{0.3}$). The as-formed cubic perovskite (respectively slightly distorted perovskite) furthermore shows a similar lattice parameter compared to the precursor oxides $Bi_{1-x}Ba_xFeO_{3-x/2}$.

We conclude that the polar tetragonal distortion is therefore very stable for the oxyfluorides $Bi_{1-x}Ba_xFeO_{3-x}F_x$, with a Curie temperature > 770 K. Structurally similar compounds (e.g., $PbTiO_3$, T_c = 760 K) show a clear decrease of the *c*/*a* ratio when approaching their Curie temperature (see, e.g., ref 97), and the fact that this is not observed for $Bi_{1-x}Ba_xFeO_{3-x}F_x$ might indicate that the tetragonal distortion is even further stabilized for those compositions.

The decomposition of the compounds at elevated temperatures and the subsequent analysis of the decomposition products can be used to prove that incorporation of F into the perovskite lattice was indeed successful (as was already shown in previous articles[64,65,62,63]). The amount of BaF_2 agrees within errors with the amount of F^- assumed in $Bi_{1-x}Ba_xFeO_{3-x}F_x$ (e.g., ∼7 wt % for $Bi_{0.8}Ba_{0.2}FeO_{2.8}F_{0.2}$). This, together with a completely filled anion sublattice indicated from the neutron data and the presence of single-valent Fe^{3+} from the Mössbauer spectroscopic characterization (see Section 3.4) provides strong evidence that a composition close to $Bi_{1-x}Ba_xFeO_{3-x}F_x$ is correct for the as-prepared oxyfluoride compounds. On decomposition at 700 °C for 5 min, we also found the formation of a rhombohedral ($R3c$) together with a cubic ($Pm\bar{3}m$) perovskite phase (in the ratio of ∼5:4). This indicates that the extraction of Ba due to the formation of BaF_2 also causes readoption of the parent rhombohedral phase for Bi-richer regions. The ratio of the cations was confirmed by EDX spectroscopy (within the errors of the method) for both compounds $Bi_{1-x}Ba_xFeO_{3-x}F_x$ (x = 0.2, 0.3), see Table 1.

3.4. Mössbauer Spectroscopy Experiments of $Bi_{0.7}Ba_{0.3}FeO_{2.7}F_{0.3}$. ^{57}Fe Mössbauer spectroscopy was measured on the compound with highest fluorine content $Bi_{0.7}Ba_{0.3}FeO_{2.7}F_{0.3}$. A single sextet (see Figure 8) with an

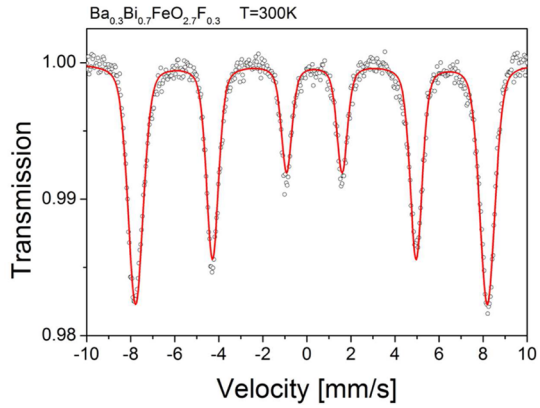

Figure 8. ^{57}Fe Mössbauer spectrum recorded from $Bi_{0.7}Ba_{0.3}FeO_{2.7}F_{0.3}$ at room temperature.

isomer shift characteristic for iron in trivalent oxidation state was found (see Table 6), and the finding of a sextet agrees well with the magnetic structure determined via neutron powder diffraction. However, to obtain a proper fit of the spectrum, a Gaussian-type distribution of magnetic fields as well as quadrupole interaction parameters had to be assumed. Such an assumption is reasonable, since due to the disorder of ions in the compound (e.g., Bi/Ba and O/F) local variations in the exact kind of ion environments will have to occur, and the fact that the quadrupole interaction parameter shows a broader distribution (compared to the distribution of the magnetic hyperfine field parameter) agrees well with this observation.

The magnetic hyperfine field parameter of 49.5 T is comparable to what was found for other magnetically ordered iron-containing perovskite compounds with Fe^{3+} being in corner-sharing octahedral coordination (e.g., $SrFeO_2F$,[59] 3C-$BaFeO_2F$,[61] 6H-$BaFeO_2F$,[63] 15R-$BaFeO_2F$[62]). Furthermore,

dx.doi.org/10.1021/ic502183t | Inorg. Chem. 2014, 53, 12572−12583

Table 6. Fitted Mössbauer Parameters for the Compound $Bi_{0.7}Ba_{0.3}FeO_{2.7}F_{0.3}$

	B_{hf}[a] (T)	ΔB_{hf}[b] (T)	ε[c] (mm/s)	$\Delta\varepsilon$[b] (mm/s)	δ_{is}[d] (mm/s)	Γ[e] (mm/s)
Fe^{3+} (O)	49.5(1)	2.1	−0.13(1)	0.4	0.285(1)	0.3[f]

[a] B_{hf} = magnetic hyperfine field. [b] ΔB_{hf} and $\Delta\varepsilon$ are Gaussian distributions of the B_{hf} and ε parameters, respectively. [c] ε = effective quadrupole interaction parameter. [d] δ_{is} = isomer shift vs α-Fe. [e] Γ = line width. [f] Γ was fixed for the fit of the pattern.

the structural characterization reported in the previous sections can also be validated by comparing the spectrum of $Bi_{0.7}Ba_{0.3}FeO_{2.7}F_{0.3}$ to data of similar compounds reported in literature. Batuk et al.[31] recorded Mössbauer data for Sr-doped $PbFeO_{2.5}$. Such lead-containing perovskite ferrites show crystallographic shearing in supposedly lead-richer regions,[30−32] which results in the formation of edge sharing between neighboring Fe polyhedra. This edge sharing is known to lower the magnetic hyperfine field interaction (e.g., to about 32 T[31] due to increased covalent interactions between the Fe and the anions, or due to possibly increased covalent Fe−Fe interactions between face-sharing octahedra as found in 6H- and 15R-$BaFeO_2F$[62,63]). Crystallographic shearing can therefore be practically ruled out for the fluorinated compounds with tetragonal distortion, since no such lowered magnetic hyperfine field parameters were found here. This holds also for the oxides due to the topochemical nature of the fluorination reaction. In addition, we could not find any doublet contributions in the Mössbauer spectrum, as was found for $Bi_{0.81}Pb_{0.19}FeO_{2.905}$,[29] or a second sextet, as was found for $Bi_{0.8}Pb_{0.2}FeO_{2.9}$, which both had been assigned to Fe with lower coordination numbers. Again, this all agrees well with a fully occupied anion lattice for the fluorinated compounds.

3.5. Magnetic Characterization of $Bi_{1-x}Ba_xFeO_{3-x/2}$ and $Bi_{1-x}Ba_xFeO_{3-x}F_x$. Field-dependent measurements of the magnetization are shown and discussed for $Bi_{0.8}Ba_{0.2}FeO_{2.9}$ and $Bi_{0.8}Ba_{0.2}FeO_{2.8}F_{0.2}$ (see inlay of Figure 9) and show a small remanent magnetization. Both compounds were shown by neutron diffraction to contain small amounts of the impurity phase $BaFe_{12}O_{19}$ of 2.0 wt % for the oxide and 1.7 wt % for the oxyfluoride. $BaFe_{12}O_{19}$ is reported to possess a remanent magnetic moment of ∼20 μ_B/f.u. (at 0 K),[98] with a high Curie temperature of 740 K. This magnetic moment could also be confirmed by the magnetic reflections of this phase present in the NPD data. We tried to correlate the observed remanent magnetization with the amount of $BaFe_{12}O_{19}$ and its known magnetic properties (see Figure 9), and we found that they agree very well within errors (which mainly arise from the quantification of this phase). This explains why the curves of the oxide and oxyfluoride are more similar for the inlay (the ideal molar masses of the oxide and oxyfluoride differ to approximately 1%) compared to the main figure, for which the magnetization had to be divided by the weight fractions of 2.0, respectively, 1.7 wt % determined for $BaFe_{12}O_{19}$. No canting of the magnetic moment of the perovskite compound needs to be assumed to explain the observed magnetic moments, and this is also in agreement with the analysis of the magnetic structures of the oxide as well as the oxyfluoride compounds reported in Sections 3.1 and 3.2.

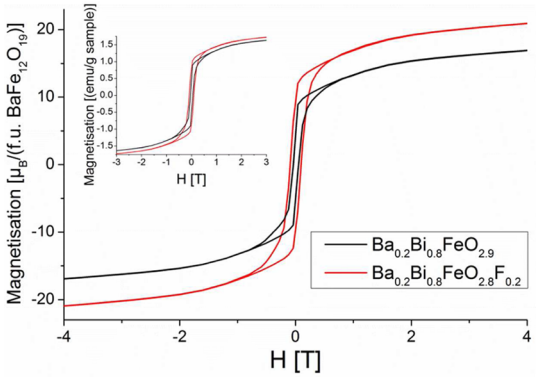

Figure 9. Field-dependent measurements of the magnetization of $Bi_{0.8}Ba_{0.2}FeO_{2.9}$ and $Bi_{0.8}Ba_{0.2}FeO_{2.8}F_{0.2}$ (inlay), measured magnetization correlated with the amount of $BaFe_{12}O_{19}$ determined by quantitative phase analysis of the NPD data.

We also found an increase for the magnetization for increasing Ba content. This is in agreement that for such increase of Ba content, an increase of the amount of $BaFe_{12}O_{19}$ was found (∼4 wt %) and can be explained by the fact that the samples had to be heated to higher temperatures for obtaining a cubic perovskite phase with nearly random distribution of Bi/Ba ions.

4. SUMMARY

In this article we have shown that tetragonal $PbTiO_3$-type $BiFeO_3$ can be stabilized by Ba doping of the Bi site and subsequent topochemical fluorination using PVDF. The as-prepared oxyfluoride compounds $Bi_{1-x}Ba_xFeO_{3-x}F_x$ contain single-valent Fe^{3+} and show a large tetragonal distortion with a c/a ratio of 1.08−1.05 (for x = 0.2/0.3) and crystallize in the polar space group $P4mm$. The compounds are isostructural to $Pb(Ti,Zr)O_3$ compounds, with similar magnitudes for the off-center displacement of the Fe ions in the octahedra as well as of the ns^2 cation Bi^{3+}. This is the first time that chemical doping was found to induce a polar tetragonal distortion in nonstressed $BiFeO_3$ compounds, which has been assumed to potentially improve switching kinetics of the compound.[36] The fluorinated compounds show G-type alignment of the magnetic moments in the a/b plane. The remanent magnetization found is in agreement with the amount of impurity of $BaFe_{12}O_{19}$, which could only be detected and quantified using neutron powder diffraction. Therefore, the intrinsic nature of the magnetic moment due to A-site doping by Ba^{2+} assumed in previous publications[80,99,68,21,25] might be questionable.

Currently techniques are being investigated to fluorinate thin films of Ba-doped $BiFeO_3$, which might then be more suitable for electrical characterization for these thermodynamically unstable compounds. The fluorination of thin epitaxially grown films of $SrFeO_{3-\delta}$ was recently reported by Moon et al.[100] and Katayama et al.[101] by the use of PVDF, and we think that this method might be, in principle, applicable to a broad range of A-site doped $Bi_{1-x}A_xFeO_{3-y}$ compounds. For such dense films, the evaluation of electric properties might then become feasible.

■ ASSOCIATED CONTENT

Supporting Information

Data are provided for the comparison of fit models using the space groups $P4mm$ and $P4/mmm$, details for Hamilton's R-test

dx.doi.org/10.1021/ic502183t | Inorg. Chem. 2014, 53, 12572−12583

comparing the structural models of $Bi_{0.7}Ba_{0.3}FeO_{2.7}F_{0.3}$ with space groups *P4mm* and *P4/mmm*, and the decomposition of $Bi_{0.7}Ba_{0.3}FeO_{2.7}F_{0.3}$ at 550 °C. Attempts to determine the electric properties of $Bi_{1-x}Ba_xFeO_{3-x/2}$ and $Bi_{1-x}Ba_xFeO_{3-x}F_x$ are also included. Structural data for the compounds $Bi_{1-x}Ba_xFeO_{3-x/2}$ and $Bi_{1-x}Ba_xFeO_{3-x}F_x$ (x = 0.2, 0.3) are provided as CIF files. This material is available free of charge via the Internet at http://pubs.acs.org.

AUTHOR INFORMATION

Corresponding Author

*Fax: +49 6151 16 6335. E-Mail: oliver.clemens@kit.edu.

Notes

The authors declare no competing financial interest.

ACKNOWLEDGMENTS

Neutron diffraction beamtime at ISIS was provided by the Science and Technology Facilities Council (STFC). H.H. appreciates the support of the State of Hesse by an equipment grant.

REFERENCES

(1) Jaffe, B.; Cook, W. R.; Jaffe, H. *Piezoelectric Ceramics;* Academic Press: London, New York, 1971.
(2) Kao, K. C. *Dielectric Phenomena in Solids;* Elsevier: Amsterdam, 2004.
(3) Newnham, R. E. *Properties of Materials: Anisotropy, Symmetry, Structure;* Oxford University Press: Oxford, 2005.
(4) Acosta, M.; Jo, W.; Rödel, J. *J. Am. Ceram. Soc.* **2014**, *97*, 1937−1943.
(5) Yao, F.-Z.; Patterson, E. A.; Wang, K.; Jo, W.; Rödel, J.; Li, J.-F. *Appl. Phys. Lett.* **2014**, *104*, 242912.
(6) Hiruma, Y.; Aoyagi, R.; Nagata, H.; Takenaka, T. *Jpn. J. Appl. Phys.* **2005**, *44*, 5040.
(7) Isupov, V. A. *Ferroelectrics* **2005**, *315*, 123−147.
(8) Shrout, T.; Zhang, S. *J. Electroceram.* **2007**, *19*, 113−126.
(9) Seifert, K. T. P.; Jo, W.; Rödel, J. *J. Am. Ceram. Soc.* **2010**, *93*, 1392−1396.
(10) Patterson, E. A.; Cann, D. P. *J. Am. Ceram. Soc.* **2012**, *95*, 3509−3513.
(11) Catalan, G.; Scott, J. F. *Adv. Mater.* **2009**, *21*, 2463−2485.
(12) Wang, J.; Neaton, J. B.; Zheng, H.; Nagarajan, V.; Ogale, S. B.; Liu, B.; Viehland, D.; Vaithyanathan, V.; Schlom, D. G.; Waghmare, U. V.; Spaldin, N. A.; Rabe, K. M.; Wuttig, M.; Ramesh, R. *Science* **2003**, *299*, 1719−1722.
(13) Neaton, J. B.; Ederer, C.; Waghmare, U. V.; Spaldin, N. A.; Rabe, K. M. *Phys. Rev. B* **2005**, *71*, 014113.
(14) Ravindran, P.; Vidya, R.; Kjekshus, A.; Fjellvåg, H.; Eriksson, O. *Phys. Rev. B* **2006**, *74*, 224412.
(15) Valant, M.; Axelsson, A.-K.; Alford, N. *Chem. Mater.* **2007**, *19*, 5431−5436.
(16) Selbach, S. M.; Einarsrud, M.-A.; Grande, T. *Chem. Mater.* **2008**, *21*, 169−173.
(17) Reitz, C.; Suchomski, C.; Weidmann, C.; Brezesinski, T. *Nano Res.* **2011**, *4*, 414−424.
(18) Liu, H.; Yang, P.; Yao, K.; Ong, K. P.; Wu, P.; Wang, J. *Adv. Funct. Mater.* **2012**, *22*, 937−942.
(19) Sosnowska, I.; Peterlin-Neumaier, T.; Steichele, E. *J. Phys. C: Solid State Phys.* **1982**, *15*, 4835−4846.
(20) Khomchenko, V. A.; Kiselev, D. A.; Vieira, J. M.; Kholkin, A. L.; Sa, M. A.; Pogorelov, Y. G. *Appl. Phys. Lett.* **2007**, *90*, 242901.
(21) Khomchenko, V. A.; Kopcewicz, M.; Lopes, A. M. L.; Pogorelov, Y. G.; Araujo, J. P.; Vieira, J. M.; Kholkin, A. L. *J. Phys. D: Appl. Phys.* **2008**, *41*, 102003.
(22) Chen, W.-t.; Williams, A. J.; Ortega-San-Martin, L.; Li, M.; Sinclair, D. C.; Zhou, W.; Attfield, J. P. *Chem. Mater.* **2009**, *21*, 2085−2093.
(23) Khomchenko, V. A.; Kiselev, D. A.; Kopcewicz, M.; Maglione, M.; Shvartsman, V. V.; Borisov, P.; Kleemann, W.; Lopes, A. M. L.; Pogorelov, Y. G.; Araujo, J. P.; Rubinger, R. M.; Sobolev, N. A.; Vieira, J. M.; Kholkin, A. L. *J. Magn. Magn. Mater.* **2009**, *321*, 1692−1698.
(24) Wang, L. Y.; Wang, D. H.; Huang, H. B.; Han, Z. D.; Cao, Q. Q.; Gu, B. X.; Du, Y. W. *J. Alloys Compd.* **2009**, *469*, 1−3.
(25) Das, R.; Mandal, K. *J. Magn. Magn. Mater.* **2012**, *324*, 1913−1918.
(26) Zhang, S.-T.; Zhang, Y.; Lu, M.-H.; Du, C.-L.; Chen, Y.-F.; Liu, Z.-G.; Zhu, Y.-Y.; Ming, N.-B.; Pan, X. Q. *Appl. Phys. Lett.* **2006**, *88*, 162901.
(27) Suresh, P.; Srinath, S. *J. Appl. Phys.* **2013**, *113*, D920.
(28) Abakumov, A. M.; Hadermann, J.; Bals, S.; Nikolaev, I. V.; Antipov, E. V.; Van Tendeloo, G. *Angew. Chem.* **2006**, *118*, 6849−6852.
(29) Dachraoui, W.; Hadermann, J.; Abakumov, A. M.; Tsirlin, A. A.; Batuk, D.; Glazyrin, K.; McCammon, C.; Dubrovinsky, L.; Van Tendeloo, G. *Chem. Mater.* **2012**, *24*, 1378−1385.
(30) Abakumov, A. M.; Batuk, M.; Tsirlin, A. A.; Tyablikov, O. A.; Sheptyakov, D. V.; Filimonov, D. S.; Pokholok, K. V.; Zhidal, V. S.; Rozova, M. G.; Antipov, E. V.; Hadermann, J.; Van Tendeloo, G. *Inorg. Chem.* **2013**, *52*, 7834−7843.
(31) Batuk, D.; Batuk, M.; Abakumov, A. M.; Tsirlin, A. A.; McCammon, C.; Dubrovinsky, L.; Hadermann, J. *Inorg. Chem.* **2013**, *52*, 10009−10020.
(32) Batuk, M.; Turner, S.; Abakumov, A. M.; Batuk, D.; Hadermann, J.; Van Tendeloo, G. *Inorg. Chem.* **2014**, *53*, 2171−2180.
(33) Bhattacharjee, S.; Pandey, D. *J. Appl. Phys.* **2010**, *107*, 124112.
(34) Christen, H. M.; Nam, J. H.; Kim, H. S.; Hatt, A. J.; Spaldin, N. A. *Phys. Rev. B* **2011**, *83*, 144107.
(35) Simões, A. Z.; Cavalcante, L. S.; Moura, F.; Longo, E.; Varela, J. A. *J. Alloys Compd.* **2011**, *509*, 5326−5335.
(36) Iliev, M. N.; Abrashev, M. V.; Mazumdar, D.; Shelke, V.; Gupta, A. *Phys. Rev. B* **2010**, *82*, 014107.
(37) Padhi, A. K.; Nanjundaswamy, K. S.; Goodenough, J. B. *J. Electrochem. Soc.* **1997**, *144*, 1188−1194.
(38) Wakihara, M. *Mater. Sci. Eng., R* **2001**, *R33*, 109−134.
(39) Islam, M. S.; Driscoll, D. J.; Fisher, C. A. J.; Slater, P. R. *Chem. Mater.* **2005**, *17*, 5085−5092.
(40) Dasgupta, S.; Das, B.; Knapp, M.; Brand, R. A.; Ehrenberg, H.; Kruk, R.; Hahn, H. *Adv. Mater.* **2014**, *26*, 4639−4644.
(41) Sanjaya Ranmohotti, K. G.; Josepha, E.; Choi, J.; Zhang, J.; Wiley, J. B. *Adv. Mater.* **2011**, *23*, 442−460.
(42) Greaves, C.; Francesconi, M. G. *Curr. Opin. Solid State Mater. Sci.* **1998**, *3*, 132−136.
(43) McCabe, E. E.; Greaves, C. *J. Fluorine Chem.* **2007**, *128*.
(44) Clemens, O.; Slater, P. R. *Rev. Inorg. Chem.* **2013**, *33*, 105−117.
(45) Al-Mamouri, M.; Edwards, P. P.; Greaves, C.; Slaski, M. *Nature (London, U.K.)* **1994**, *369*, 382−384.
(46) Al-Mamouri, M.; Edwards, P. P.; Greaves, C.; Slater, P. R.; Slaski, M. *J. Mater. Chem.* **1995**, *5*, 913−916.
(47) Hirai, D.; Climent-Pascual, E.; Cava, R. J. *Phys. Rev. B* **2011**, 84.
(48) Romero, F. D.; Bingham, P. A.; Forder, S. D.; Hayward, M. A. *Inorg. Chem.* **2013**, *52*, 3388−3398.
(49) Luo, K.; Tran, T. T.; Halasyamani, P. S.; Hayward, M. A. *Inorg. Chem.* **2014**, *52*, 13762−13769.
(50) Saratovsky, I.; Lockett, M. A.; Rees, N. H.; Hayward, M. A. *Inorg. Chem.* **2008**, *47*, 5212−5217.
(51) Ehora, G.; Renard, C.; Daviero-Minaud, S.; Mentré, O. *Chem. Mater.* **2007**, *19*, 2924−2926.
(52) Mentré, O.; Kabbour, H.; Ehora, G.; Tricot, G. g.; Daviero-Minaud, S.; Whangbo, M.-H. *J. Am. Chem. Soc.* **2010**, *132*, 4865−4875.
(53) Sturza, M.; Daviero-Minaud, S.; Kabbour, H.; Gardoll, O.; Mentré, O. *Chem. Mater.* **2010**, *22*, 6726−6735.
(54) Sturza, M.; Daviero-Minaud, S.; Huvé, M.; Renaut, N.; Tiercelin, N.; Mentré, O. *Inorg. Chem.* **2011**, *50*, 12499−12507.

(55) Sturza, M.; Kabbour, H.; Daviero-Minaud, S.; Filimonov, D.; Pokholok, K.; Tiercelin, N.; Porcher, F.; Aldon, L.; Mentré, O. *J. Am. Chem. Soc.* **2011**, *133*, 10901−10909.
(56) Slater, P. R. *J. Fluorine Chem.* **2002**, *117*, 43−45.
(57) Clemens, O.; Rongeat, C.; Anji Reddy, M.; Giehr, A.; Fichtner, M.; Hahn, H. *Dalton Trans.* **2014**, *43*, 15771−15778.
(58) Berry, F. J.; Ren, X.; Heap, R.; Slater, P.; Thomas, M. F. *Solid State Commun.* **2005**, *134*, 621−624.
(59) Berry, F. J.; Heap, R.; Helgason, Ö.; Moore, E. A.; Shim, S.; Slater, P. R.; Thomas, M. F. *J. Phys.: Condens. Matter* **2008**, *20*, 215207.
(60) Heap, R.; Slater, P. R.; Berry, F. J.; Helgason, O.; Wright, A. J. *Solid State Commun.* **2007**, *141*, 467−470.
(61) Berry, F. J.; Coomer, F. C.; Hancock, C.; Helgason, Ö.; Moore, E. A.; Slater, P. R.; Wright, A. J.; Thomas, M. F. *J. Solid State Chem.* **2011**, *184*, 1361−1366.
(62) Clemens, O.; Berry, F. J.; Bauer, J.; Wright, A. J.; Knight, K. S.; Slater, P. R. *J. Solid State Chem.* **2013**, *203*, 218−226.
(63) Clemens, O.; Wright, A. J.; Berry, F. J.; Smith, R. I.; Slater, P. R. *J. Solid State Chem.* **2013**, *198*, 262−269.
(64) Clemens, O.; Haberkorn, R.; Slater, P. R.; Beck, H. P. *Solid State Sci.* **2010**, *12*, 1455−1463.
(65) Clemens, O.; Kuhn, M.; Haberkorn, R. *J. Solid State Chem.* **2011**, *184*, 2870−2876.
(66) Clemens, O.; Berry, F. J.; Wright, A. J.; Knight, K. S.; Perez-Mato, J. M.; Igartua, J. M.; Slater, P. R. *J. Solid State Chem.* **2013**, *206*, 158−169.
(67) Hancock, C. A.; Herranz, T.; Marco, J. F.; Berry, F. J.; Slater, P. R. *J. Solid State Chem.* **2012**, *186*, 195−203.
(68) Khomchenko, V. A.; Kiselev, D. A.; Seluneva, E. K.; Vieira, J. M.; Lopes, A. M. L.; Pogorelov, Y. G.; Araujo, J. P.; Kholkin, A. L. *Mater. Lett.* **2008**, *62*, 1927−1929.
(69) Khomchenko, V. A.; Kiselev, D. A.; Vieira, J. M.; Jian, L.; Kholkin, A. L.; Lopes, A. M. L.; Pogorelov, Y. G.; Araujo, J. P.; Maglione, M. *J. Appl. Phys.* **2008**, *103*, 024105.
(70) Coelho, A. A. TOPAS-Academic. http://www.topas-academic.net (last accessed: 20th of October 2014).
(71) *Topas V4.2*,, General profile and structure analysis software for powder diffraction data, User's Manual; Bruker AXS: Karlsruhe, Germany, 2008.
(72) Brand, R. A.; Lauer, J.; Herlach, D. M. *J. Phys. F: Met. Phys.* **1983**, *13*, 675.
(73) Boullay, P.; Grebille, D.; Hervieu, M.; Raveau, B.; Suard, E. *J. Solid State Chem.* **1999**, *147*, 450−463.
(74) Boullay, P.; Hervieu, M.; Nguyen, N.; Raveau, B. *J. Solid State Chem.* **1999**, *147*, 45−57.
(75) Jovalekić, Č.; Zdujić, M.; Poleti, D.; Karanović, L.; Mitrić, M. *J. Solid State Chem.* **2008**, *181*, 1321−1329.
(76) Conflant, P.; Boivin, J. C.; Nowogrocki, G.; Thomas, D. *Solid State Ionics* **1983**, *9−10* (Part 2), 925−928.
(77) Collomb, A.; Wolfers, P.; Obradors, X. *J. Magn. Magn. Mater.* **1986**, *62*, 57−67.
(78) Kreisel, J.; Vincent, H.; Tasset, F.; Wolfers, P. *J. Magn. Magn. Mater.* **2000**, *213*, 262−270.
(79) Clemens, O.; Gröting, M.; Witte, R.; Perez-Mato, J. M.; Loho, C.; Berry, F. J.; Kruk, R.; Knight, K. S.; Wright, A. J.; Hahn, H.; Slater, P. R. *Inorg. Chem.* **2014**, *53*, 5911−5921.
(80) Wang, D. H.; Goh, W. C.; Ning, M.; Ong, C. K. *Appl. Phys. Lett.* **2006**, *88*.
(81) Kubel, F.; Schmid, H. *Acta Crystallogr.* **1990**, *B46*, 698−702.
(82) Hoppe, R. *Angew. Chem.* **1959**, *71*, 457−457.
(83) Harada, J.; Pedersen, T.; Barnea, Z. *Acta Crystallogr.* **1970**, *26*, 336−344.
(84) Reitz, C.; Leufke, P. M.; Hahn, H.; Brezesinski, T. *Chem. Mater.* **2014**, *26*, 2195−2202.
(85) Sani, A.; Hanfland, M.; Levy, D. *J. Solid State Chem.* **2002**, *167*, 446−452.
(86) Hamilton, W. *Acta Crystallogr.* **1965**, *18*, 502−510.
(87) Cohen, R. E. *Nature* **1992**, *358*, 136−138.
(88) Hyde, B. G.; Andersson, S. *Inorganic Crystal Structures;* John Wiley: New York, 1989.
(89) Walsh, A.; Watson, G. W.; Payne, D. J.; Edgell, R. G.; Guo, J.; Glans, P.-A.; Learmonth, T.; Smith, K. E. *Phys. Rev. B* **2006**, *73*, 235104.
(90) Shannon, R. D. *Acta Crystallogr.* **1976**, *A32*, 751−767.
(91) Holleman, A. F.; Wiberg, N. *Lehrbuch der Anorganischen Chemie, 101. Auflage;* deGruyter: Berlin, 1995.
(92) MAXMAGN in the Bilbao Crystallographic Server. http://cryst.ehu.es (last accessed: 20th of October 2014),.
(93) Aroyo, M. I.; Kirov, A.; Capillas, C.; Perez-Mato, J. M.; Wondratschek, H. *Acta Crystallogr.* **2006**, *A62*, 115−128.
(94) Aroyo, M. I.; Perez-Mato, J. M.; Capillas, C.; Kroumova, E.; Ivantchev, S.; Madariaga, G.; Kirov, A.; Wondratschek, H. *Z. Kristallogr.* **2006**, *221*, 15−27.
(95) Aroyo, M. I.; Perez-Mato, J. M.; Orobengoa, D.; Tasci, E.; de la Flor, G.; Kirov, A. *Bulg. Chem. Commun.* **2011**, *43*, 183−197.
(96) Kisi, E. H.; Howard, C. J. *Applications of Neutron Powder Diffraction;* Oxford University Press: New York, 2008.
(97) Sai Sunder, V. V. S. S.; Halliyal, A.; Umarji, A. M. *J. Mater. Res.* **1995**, *10*, 1301−1306.
(98) Coey, J. M. D. *Magnetism and Magnetic Materials;* Cambridge University Press: Cambridge, 2009.
(99) Meiya, L.; Min, N.; Yungui, M.; Qibin, W.; Ong, C. K. *J. Phys. D: Appl. Phys.* **2007**, *40*, 1603.
(100) Moon, E. J.; Xie, Y.; Laird, E. D.; Keavney, D. J.; Li, C. Y.; May, S. J. *J. Am. Chem. Soc.* **2014**, *136*, 2224−2227.
(101) Katayama, T.; Chikamatsu, A.; Hirose, Y.; Takagi, R.; Kamisaka, H.; Fukumura, T.; Hasegawa, T. *J. Mater. Chem. C* **2014**, *2*, 5350−5356.